Supporting Information

Ligand-Amplified Quantum Tunneling in Polymer-Mediated Artificial Photosystems

Peng Su, Si-Han Lin, Fang-Xing Xiao*

College of Materials Science and Engineering, Fuzhou University, New Campus, Minhou, Fujian Province, 350108, China.

E-mail: fxxiao@fzu.edu.cn

Table of Contents

Page NO.

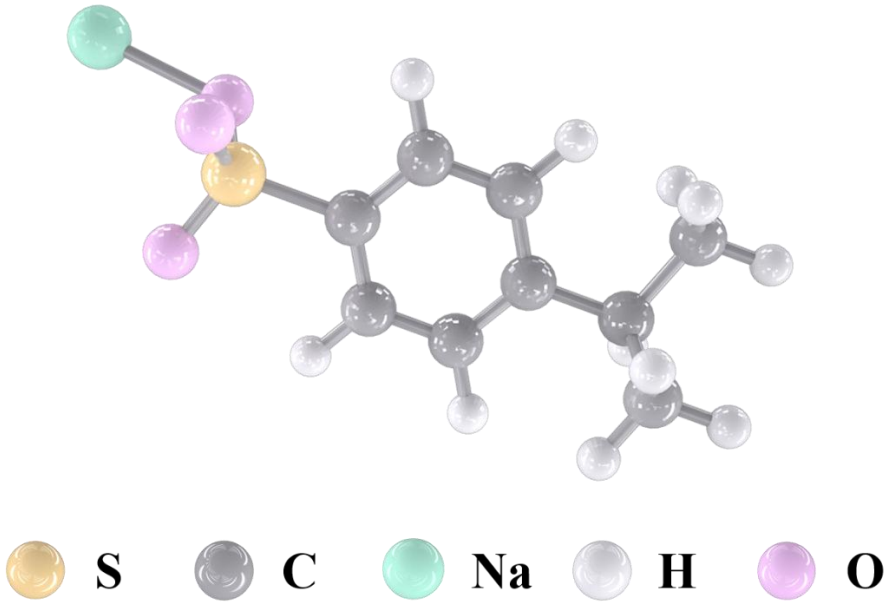

Figure S1. Molecular structure of PSS.

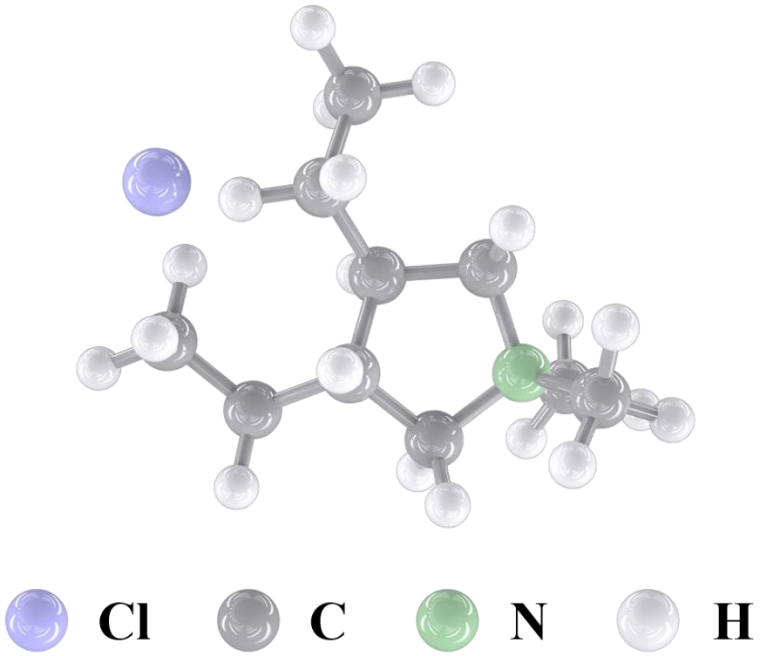

Figure S2. Molecular structure of PDDA.

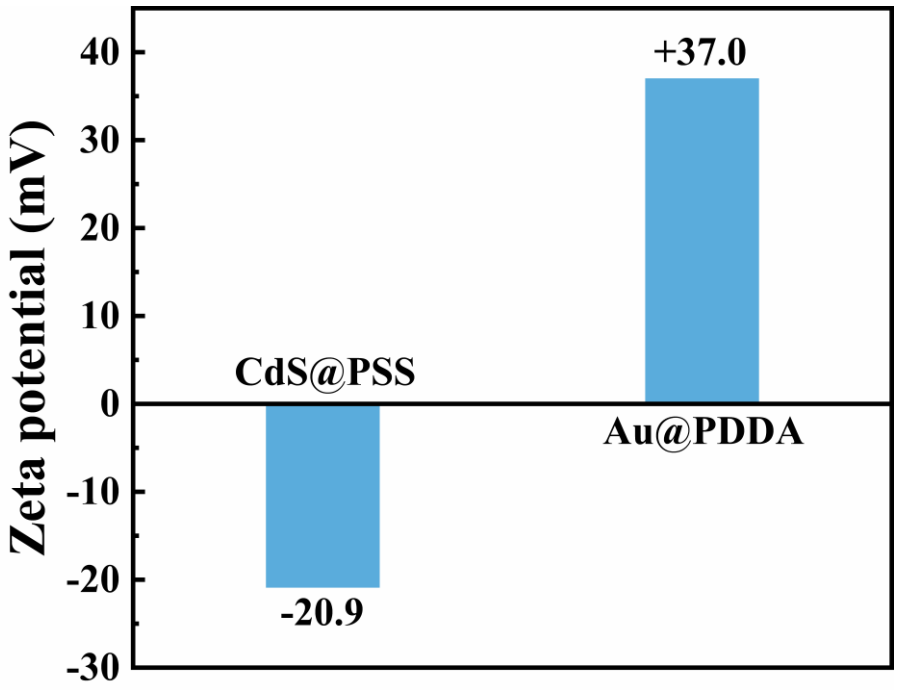

Figure S3. Zeta potentials (ξ) of CdS@PSS and Au@PDDA.

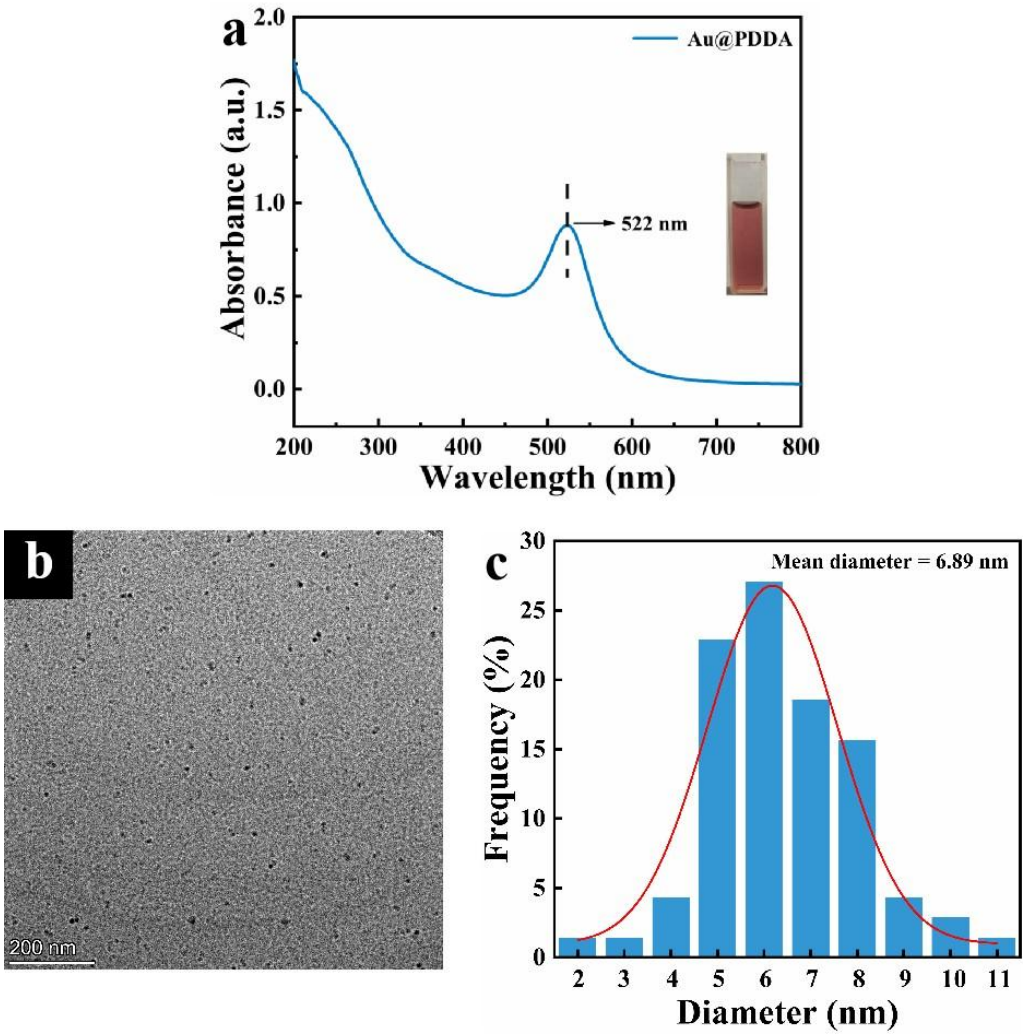

Figure S4. (a) UV-vis absorption spectrum of Au@PDDA NCs with photograph in the inset. (b) TEM image of Au@PDDA with (c) size distribution histogram.

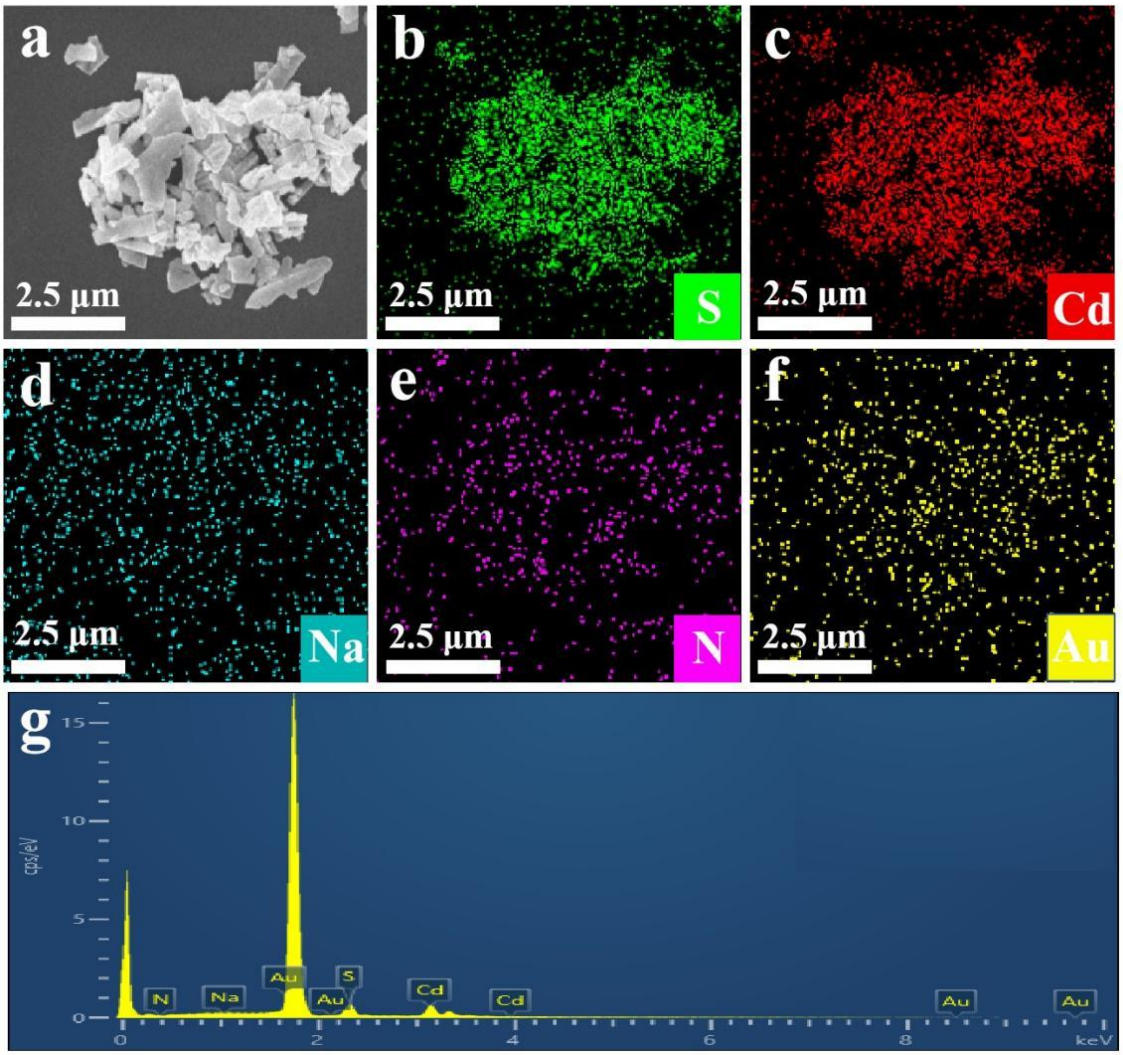

Figure S5. (a) SEM image of C@P/Au-0.25, (b-f) elemental mapping and (g) EDS results.

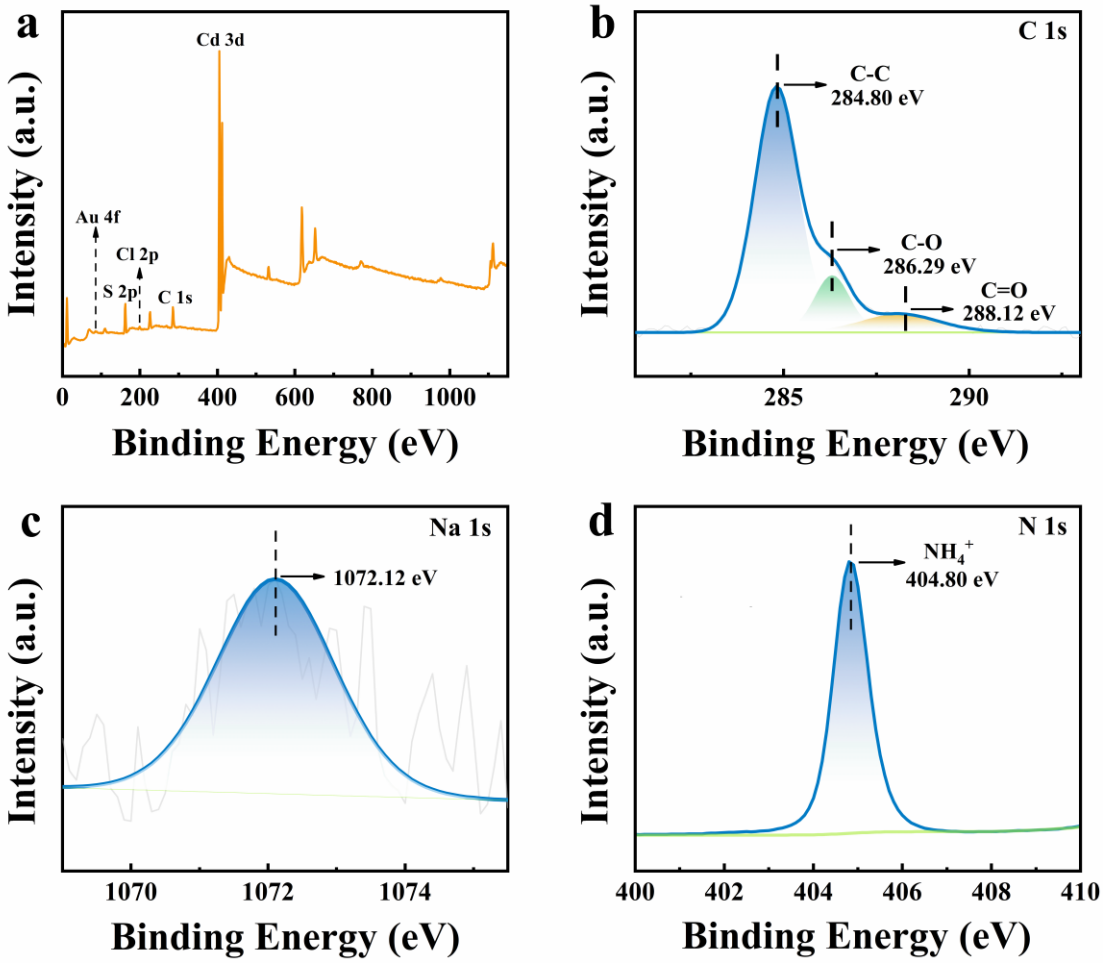

Figure S6. (a) Survey spectra and high-resolution (b) C 1s, (c) Na 1s and (d) N 1s spectra of C@P/Au-0.25.

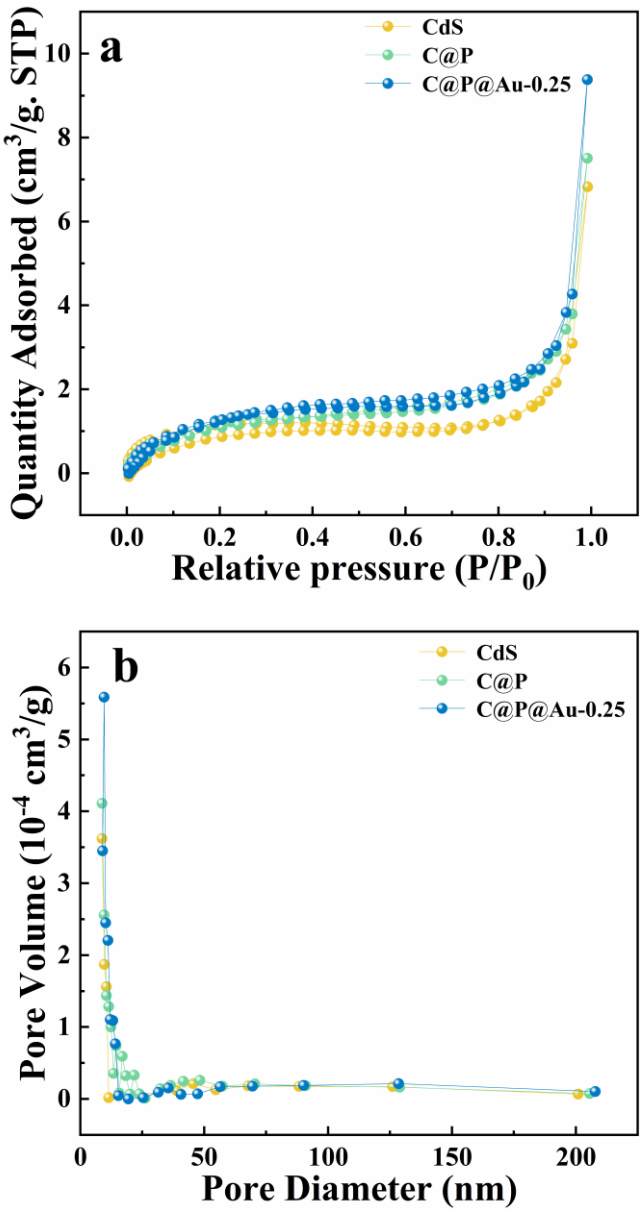

Figure S7. (a) N_2 adsorption-desorption isotherms and (b) pore size distribution curves (inset) of CdS, C@P and C@P/Au-0.25.

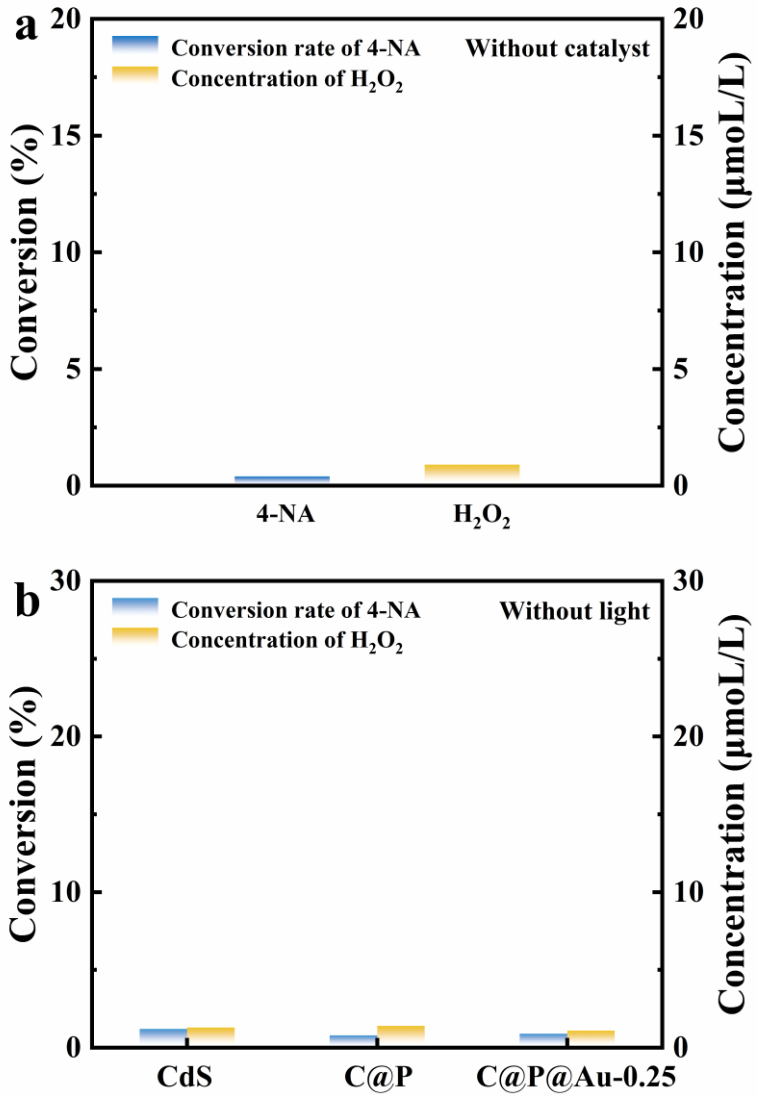

Figure S8. The conversion rate of 4-NA and the concentration of H_2O_2 under (a) catalyst-free and (b) light-free irradiation conditions in the visible light irradiation system.

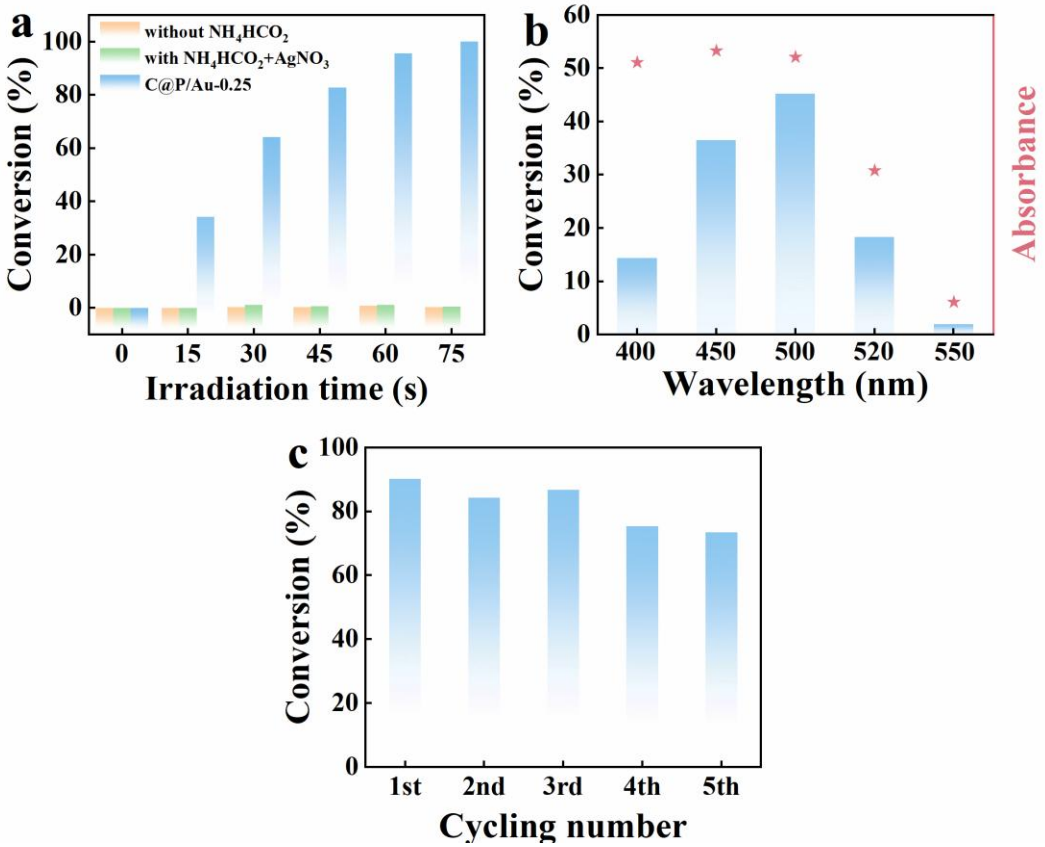

Figure S9. Photocatalytic performances of C@P/Au-0.25 toward selective reduction of 4-NA (a) in the presence of different sacrificial reagents, (b) under different monochromatic light irradiation and the corresponding UV-Vis absorbance (asterisks), (c) cyclic reaction of C@P/Au-0.25 toward 4-NA photoreduction.

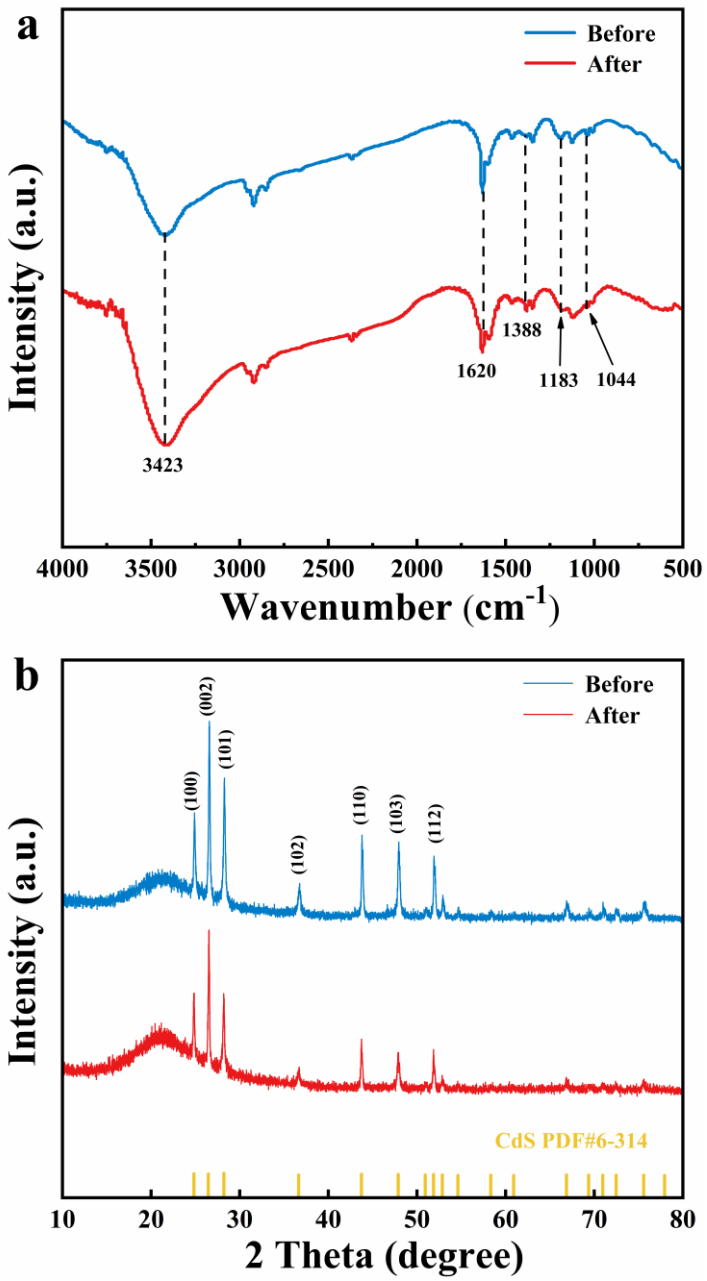

Figure S10. (a) FTIR spectra and (b) XRD patterns of C@P/Au-0.25 before and after cyclic reactions toward 4-NA photoreduction.

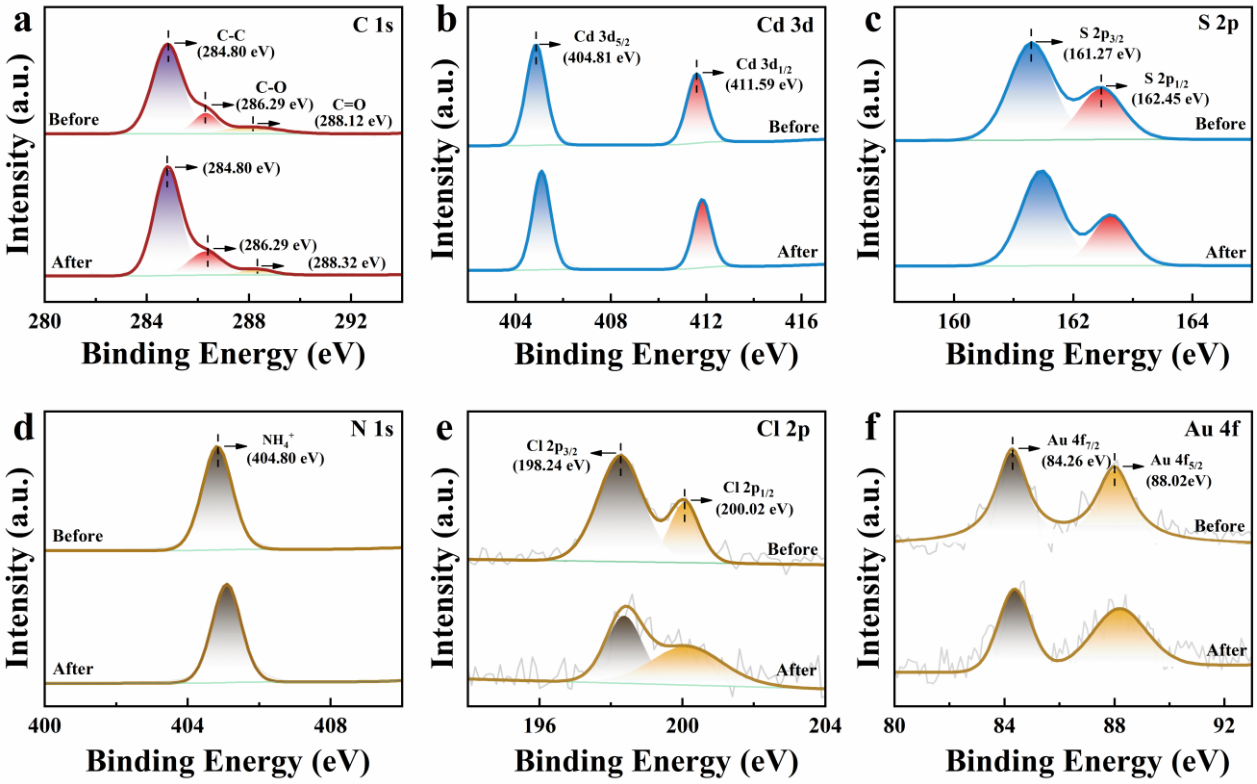

Figure S11. High-resolution (a) C1s, (b) Cd 3d, (c) S2p, (d) N1s, (e) Cl 2p and (f) Au 4f spectra of C@P/Au-0.25 before and after cyclic reactions toward 4-NA photoreduction.

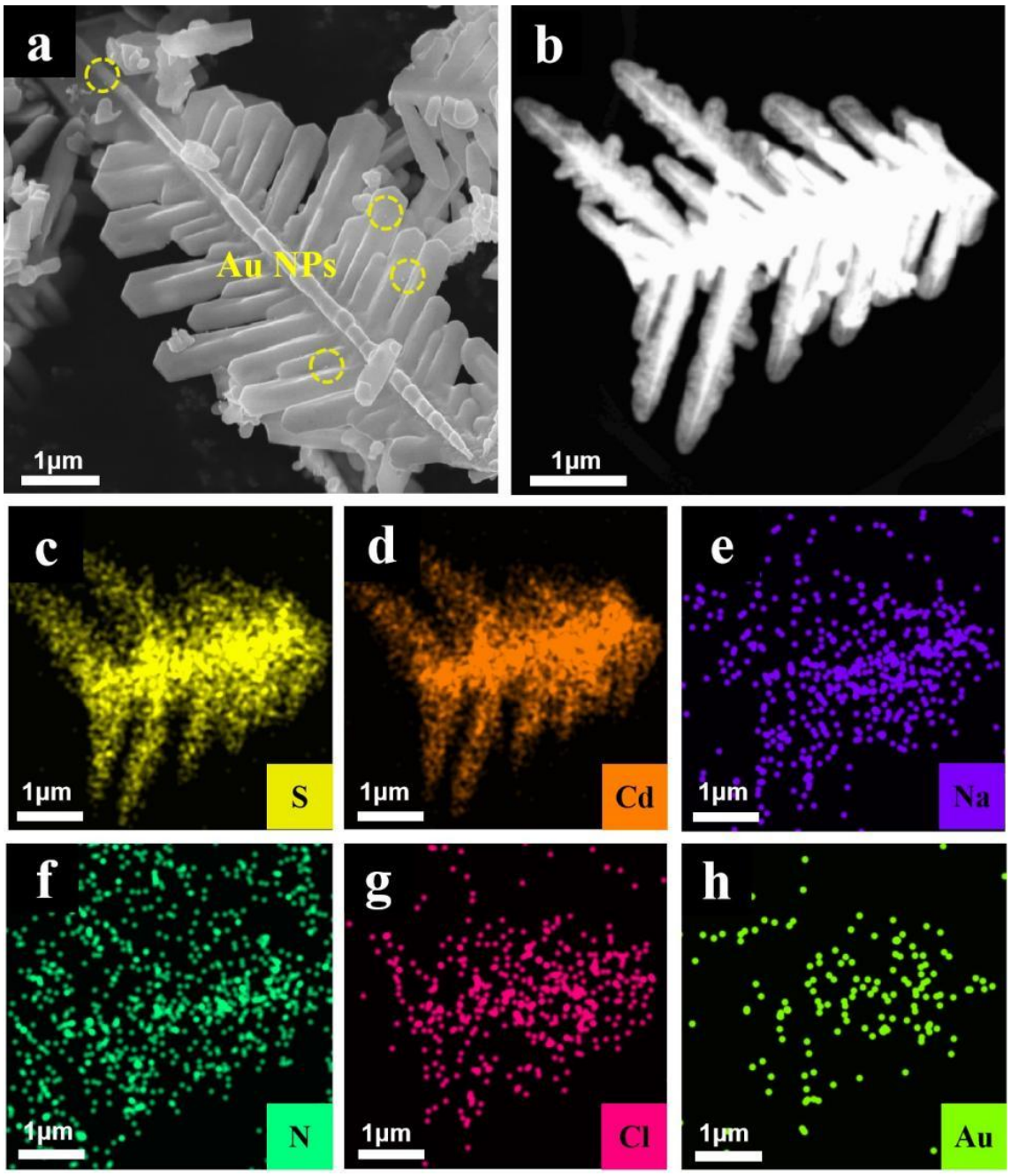

Figure S12. (a) SEM image, (b-h) TEM elemental mapping results of C@P/Au-0.25 after cyclic reactions toward 4-NA photoreduction.

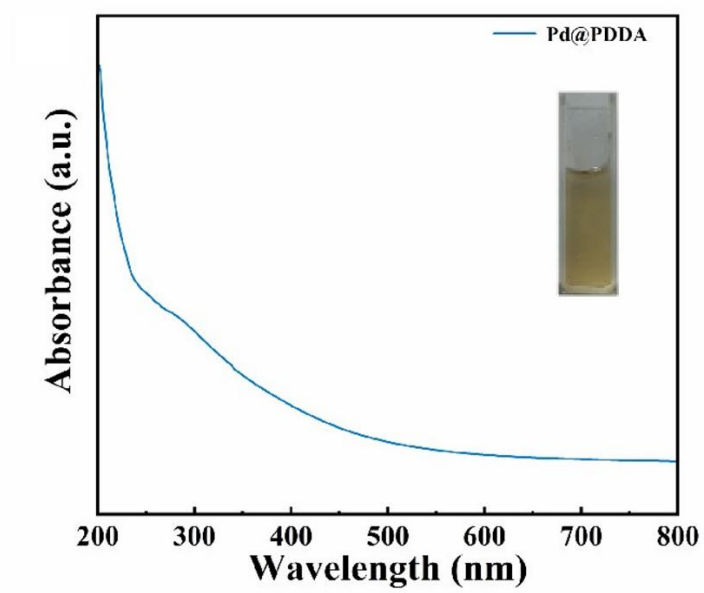

Figure S13. (a) UV-vis absorption spectrum of Pd@PDDA NCs with photograph in the inset.

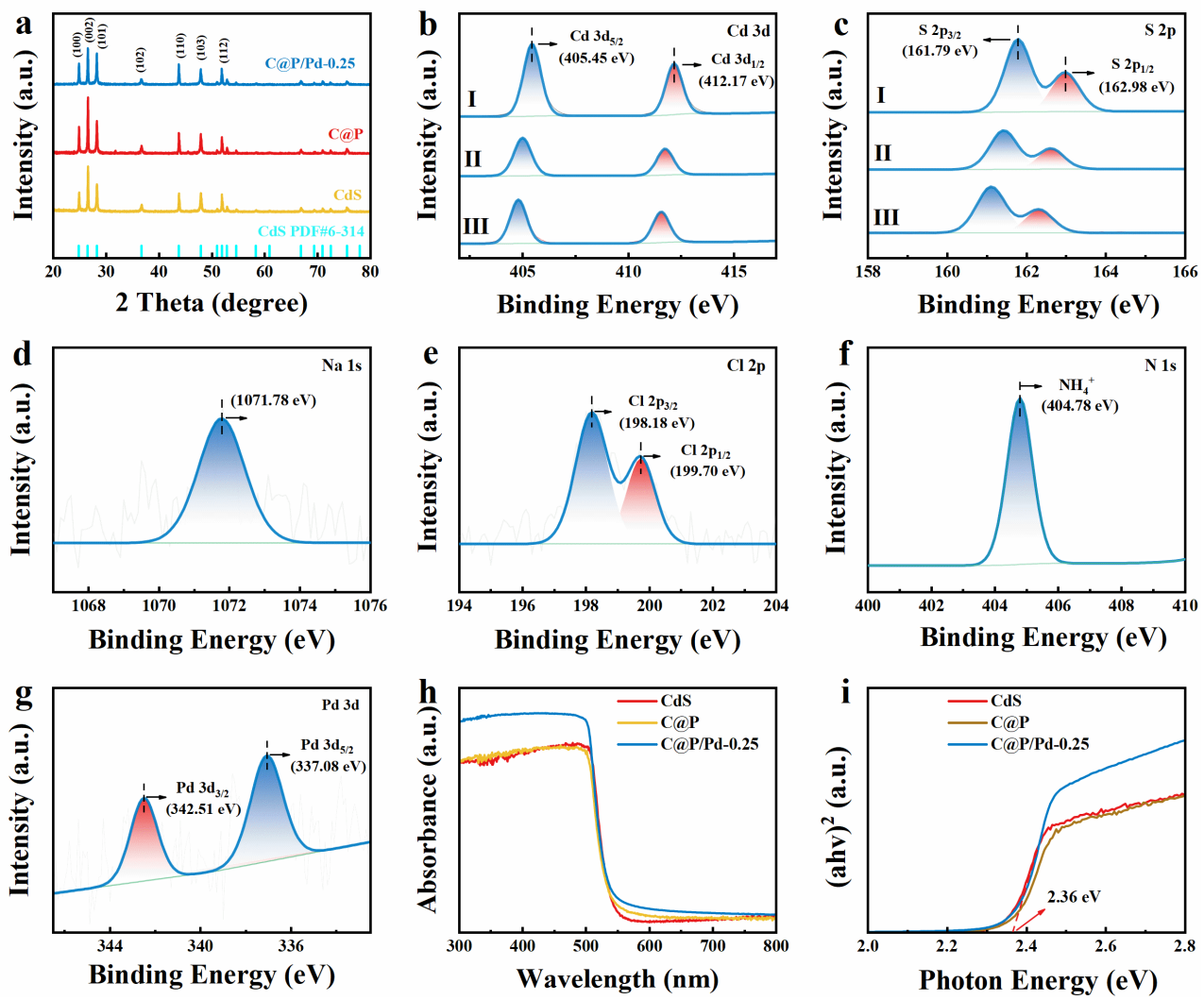

Figure S14. (a) XRD patterns of CdS, C@P and C@P15/Pd-0.25. High-resolution (b) Cd 3d and (c) S 2p spectra of (I) pristine CdS, (II) C@P and (III) C@P/Pd-0.25. High-resolution (d) Na 1s, (e) Cl 2p, (f) N 1s and (g) Pd 3d spectra of C@P@Pd-0.25. (h) DRS results of CdS, C@P, and C@P/Pd-0.25 with (i) transformed plots based on the Kubelka-Munk function vs. energy of light.

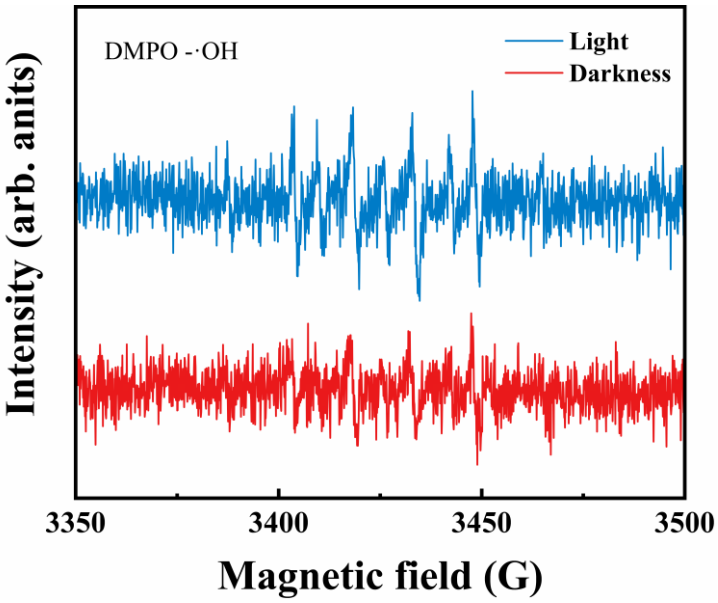

Figure S15. EPR spectra of ·OH generated by C@P/Au-0.25 under light and dark conditions.

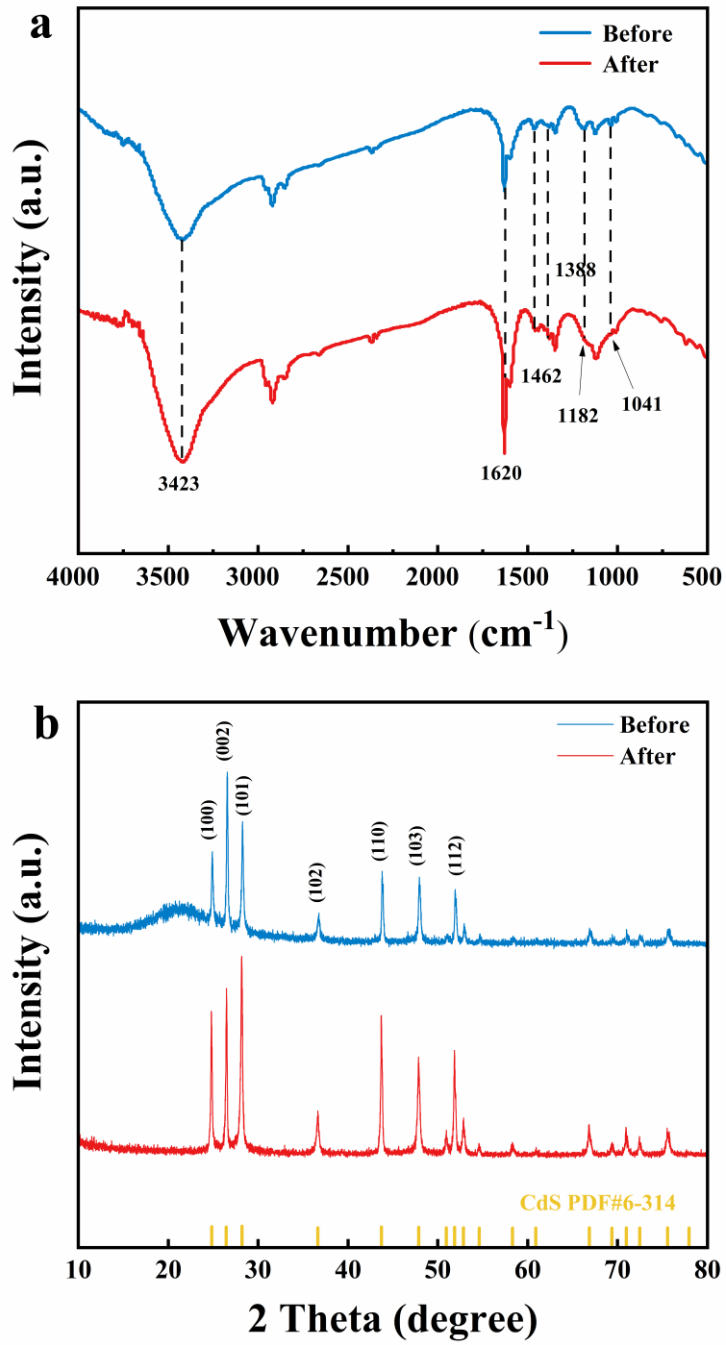

Figure S16. (a) FTIR spectra and (b) XRD patterns of C@P/Au-0.25 before and after cyclic reactions for photocatalytic H_2O_2 generation.

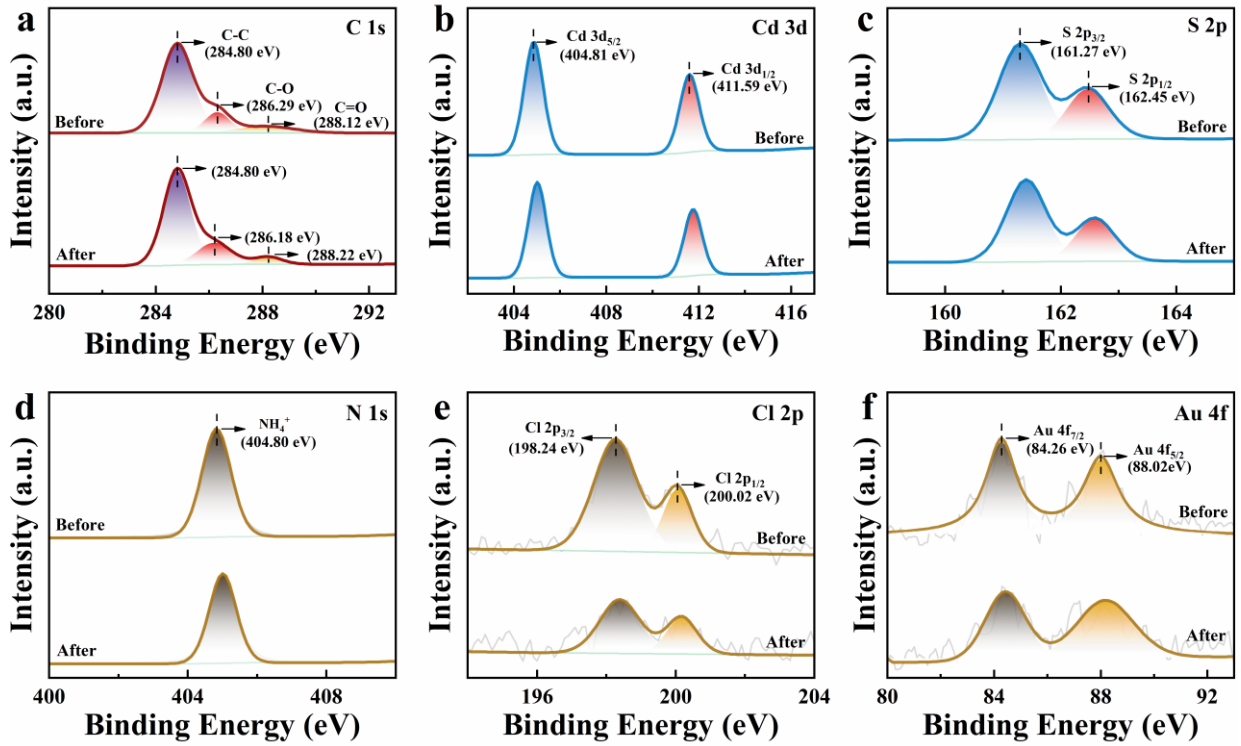

Figure S17. High-resolution (a) C1s, (b) Cd 3d, (c) S2p, (d) N1s, (e) Cl 2p and (f) Au 4f spectra of C@P/Au-0.25 before and after cyclic reactions for photocatalytic H_2O_2 generation.

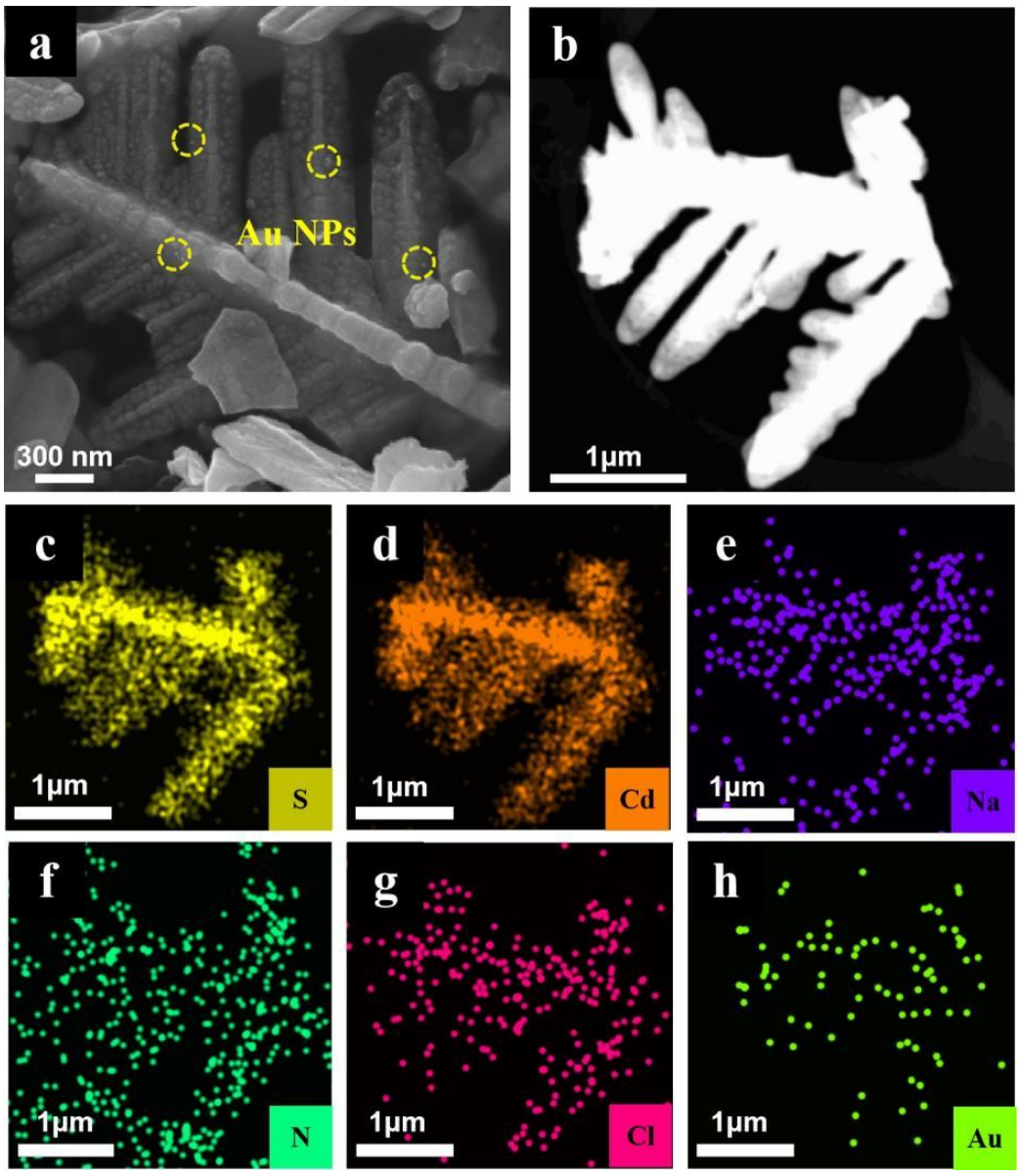

Figure S18. (a) SEM image, (b-h) TEM elemental mapping results of C@P/Au-0.25 after cyclic reactions for photocatalytic H_2O_2 generation.

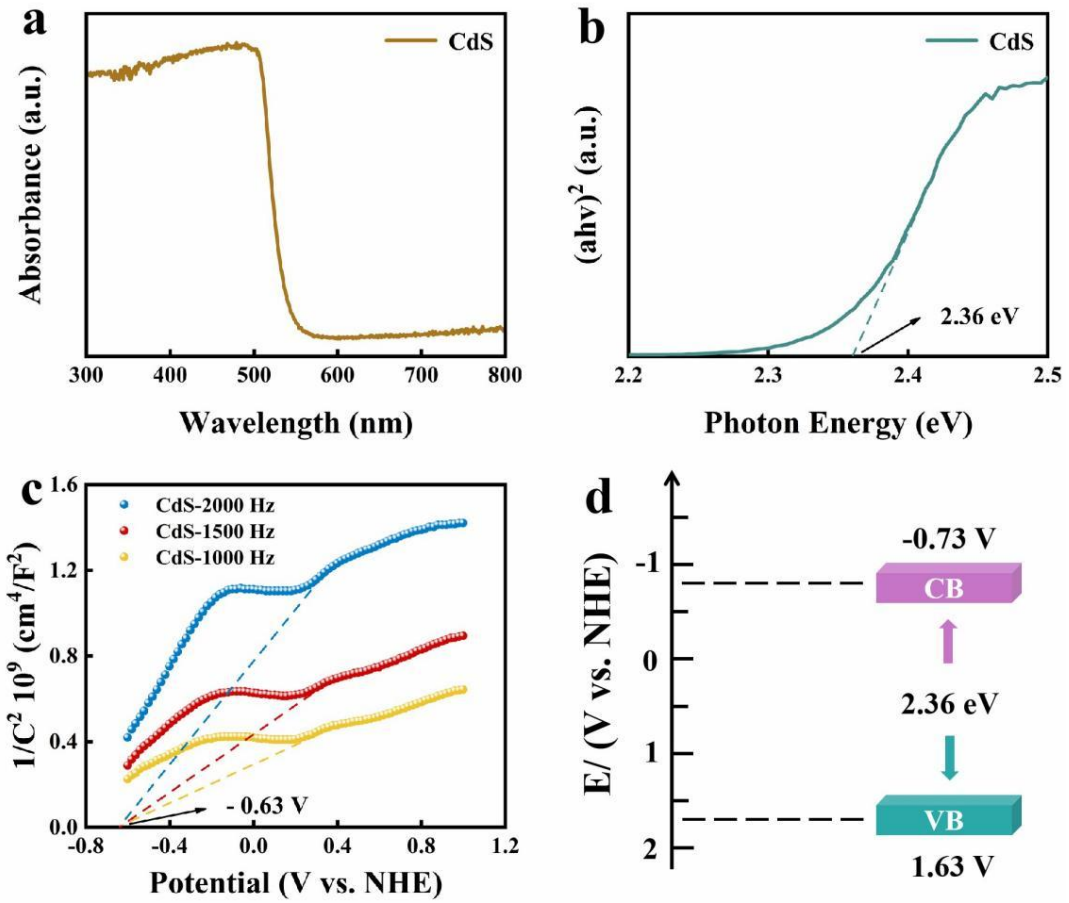

Figure S19. (a) DRS results of CdS with (b) transformed plots based on the Kubelka-Munk function vs. energy of light. (c) Mott-Schottky plots of CdS and (d) schematic diagram of energy level alignment of CdS.

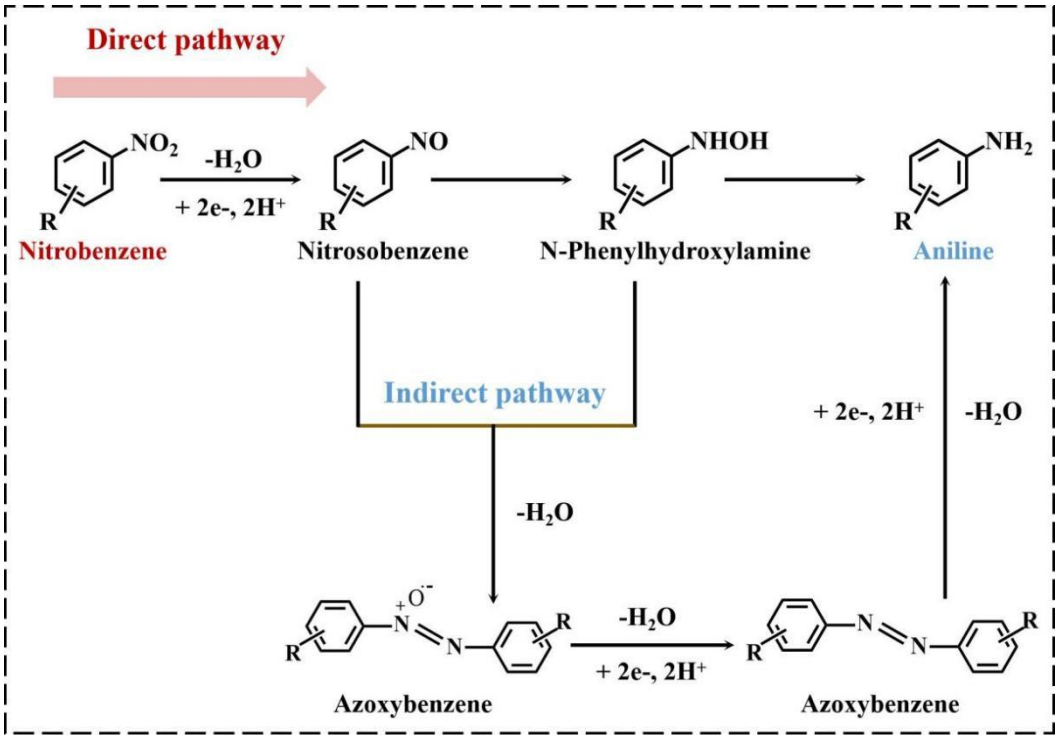

Figure S20. Photocatalytic mechanism of hydrogenation of nitroaromatics.

Note: According to previous studies, photocatalytic reduction of aromatic nitro compounds may proceed through two possible pathways: a direct route and an indirect route.[1] In the direct route, nitrobenzene (Ph-NO_2) undergoes three consecutive hydrogenation steps, ultimately yielding aniline (Ph-NH_2). The indirect route involves the condensation of nitrosobenzene (Ph-N=NO-Ph), followed by sequential formation of an azo compound (R-N=N-R), a hydrazo compound (R-NH-NH-R), and finally aniline.

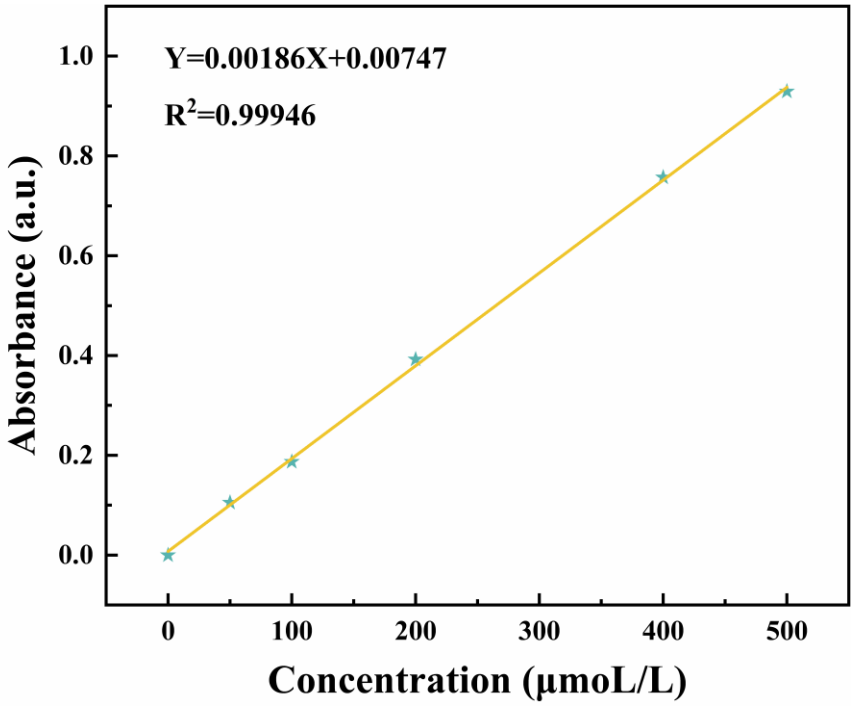

Figure S21. The standard calibration curve of H_2O_2 generation.

Table S1. Peak position with corresponding functional groups.

Peak position (cm^{-1})	Vibrational mode	Functional groups
1038 & 1182		$-SO_3$ [2, 3]
1381	δ_{C-H}	-CH- & $-CH_3$ [4]
1462	δ_{C-H}	$-CH_2$ [5]
1620	δ_{O-H}	O-H [4]
3432	V_{O-H}	O-H [4]

Table S2. Chemical bond species vs. B.E. for CdS, C@P andC@P/Au-0.25.

Element	CdS	C@P	C@P/Au-0.25	Chemical bond species
S $2p_{3/2}$	161.79	161.43	161.27	S^{2-} [6]
S $2p_{1/2}$	162.98	162.62	162.45	S^{2-} [6]
Cd $3d_{5/2}$	405.45	405.00	404.81	Cd^{2+} [7]
Cd $3d_{3/2}$	412.17	411.75	411.59	Cd^{2+} [7]
C 1s	284.80	284.80	284.80	C-C [8]
C 1s	286.59	286.25	286.14	C-O [8]
C 1s	288.88	288.20	288.12	C=O [8]
Cl $2p_{3/2}$	None	None	198.24	Cl^{-} [7]
Cl $2p_{1/2}$	None	None	200.02	Cl^{-} [7]
N 1s	None	None	404.80	NH^{4+} [9]
Au $4f_{7/2}$	None	None	84.26	Au^{0} [10]
Au $4f_{5/2}$	None	None	88.02	Au^{0} [10]

Table S3. Summary of specific surface area, pore volume and pore size of CdS, C@P and C@P/Au-0.25.

Samples	S_{BET} (m^2 g^{-1})[a]	Total pore volume (cm^3 g^{-1})[b]	Average pore size (nm)[c]
CdS	3.803	0.004	3.876
C@P	3.952	0.005	4.832
C@P/Au-0.25	4.871	0.005	4.175

[a] BET surface area is calculated from the linear part of BET plot.

[b] Single point total pore volume of the pores at P/P0 = 0.95.

[c] Adsorption average pore width (4V/A by BET).

Table S4. Comparison of the photocatalytic selective reduction of 4-NA in this work with previously reported CdS-based photocatalytic systems.

Number	***Materials***	***Sphere***	***Light source***	***Conversion (%)***	***Reference***
This work	TMC@PSS/M@PDDA	nano-leaf	Visible light (λ > 420 nm)	4-NA (100%)	/
1	CdS-NP	nanoparticles	blue LED (λ ⩾ 420 nm)	4-NA (70%)	Chem. Pap., 2016, 70, 531-537.
2	4-CdS/CeO_2	nanowires	Visible light (λ > 420 nm)	4-NP (93.3%)	J. Alloys Compd., 2021, 885, 160961.
3	CdTe QDs/5%GR	nanosheets	Visible light (λ > 420 nm)	4-NA (59.8%)	Inorg. Chem., 2020, 59, 16654-16664.
4	CdS-In120	hexagrams	Visible light (λ = 420-800 nm)	4-NA (99.4%)	J. Colloid Interface Sci., 2021, 601, 186-195.
5	CdS/Ag_2S	nanorod	Visible light (λ > 420 nm)	4-NA (99.6%)	Inorg. Chem. 2025, 64, 19413-19422.
6	5%GR-CdS	nanosheets	Visible light (λ > 420 nm)	2-NA (77%)	J. Energy Chem., 2014, 23, 145-155.
7	C@P1/A1	nano-leaves	Visible light (λ > 400 nm)	Nitrobenzene (85%)	Chem. Sci., 2024,15, 10625-10637.
8	$ZC^{0.5}A^{1}$	dendritic structure	Visible light (λ > 400 nm)	4-NA (99.5%)	J. Catal., 2022, 410, 31-41.

Table S5. Comparison of the photocatalytic H_2O_2 production in this work with previously reported CdS-based photocatalytic systems.

Number	***Materials***	***Sphere***	***Light source***	***Activity (μmol/g/h)***	***Reference***
This work	TMC@PSS/M@PDDA	nano-leaf	Visible light (λ > 420 nm)	2513.42	/
1	CdS/rGO	nanoparticles	blue LED (λ > 420 nm)	290.3	Appl. Catal. B Environ. Energy, 2019, 241, 367-374.
2	CdS-NR	nanoflower	Visible light (λ > 420 nm)	1225.1	Chinese Journal of Chemical, 2026, 89, 259-266.
3	CdS-Mn-G	nanoparticles	300 W xenon lamp	1874	Inorg. Chem. Front., 2025,12, 5177-5188.
4	CdS-rGO@AQS	nanoparticles	Visible light (λ = 420-800 nm)	1331	Ind. Eng. Chem. Res. 2023, 62, 12974-12984
5	CdS/Ag_2S	nanorod	AM1.5	1620	Small. 2024, 20, 2400376.
6	$CdS/K_2Ta_2O_6$	spherical structure	Visible light (λ > 420 nm)	160.89	Chem. Eng. J. 2023, 452, 139070.
7	CdS/RF	spheres	Visible light (λ > 400 nm)	2136	J. Mater. Sci. Technol., 2023,162, 90-98.
8	C-CdS	pine-leaf-like	Visible light (λ > 420 nm)	204.17	Chem. Eng. J., 2022, 450, 138024.
9	CT-0.5	nanosheets	Visible light (λ > 400 nm)	802	ACS Appl. Nano Mater., 2023, 6, 558-572.

Table S6. Fitted EIS results of different samples under visible light irradiation based on the equivalent circuit.

Samples	Rs/ohm	Rct/ohm	CPE/(10^{-5} F cm^{-2})
C@P	18.48	18930	6.753
C@P@Au-0.25	18.10	8548	6.118

Note: As shown in **Table S4**, Rct values were obtained by fitting the EIS results according to a simple equivalent circuit composed of a series of resistance (Figure 6b, inset). Apparently, C@P@Au-0.25 demonstrates the smallest Rct value in comparison with other counterparts, indicative its lowest interfacial charge transfer resistance.

References

1. H. Liang, B. J. Liu, B. Tang, S. C. Zhu, S. Li, X. Z. Ge, J. L. Li, J. R. Zhu and F. X. Xiao, Atomically precise metal nanocluster-mediated photocatalysis, *ACS Catal.*, 2022, **12**, 4216-4226.
2. A. F. Elerian, A. A. Mohamed, E. M. Elnaggar, G. Abdel-Naeem and M. A. Abu-Saied, Investigation on sulfonated PVC/polymethyl methacrylate (PMMA)/polystyrene sulfonate (PSS) polymer blends as proton-conducting membrane, *Polym. Bull.*, 2024, **81**, 17177-17212.
3. J. V. Antony, P. Kurian, N. P. N. Vadakkedathu and G. E. Kochimoolayil, In situ synthesis of CdS quantum dot-partially sulfonated polystyrene composite: characterization and optical properties, *Ind. Eng. Chem. Res.*, 2014, **53**, 2261-2269.
4. S. Xu, M. H. Huang, T. Li, Z. Q. Wei, X. Lin, X. C. Dai, S. Hou, X. Y. Fu and F. X. Xiao, Modulating charge migration in photoredox organic transformation via exquisite interface engineering, *J. Mater. Chem. A*, 2020, **8**, 8360-8375.
5. R. S. Jing, J. S. Yang, S. T. Li, S. F. Zhao, P. F. Wang, Y. Y. Liu, A. J. Liu, Z. L. Meng, H. W. Huang, Z. L. Zhang and Q. Zhang, Construction of PDDA functionalized black phosphorus nanosheets/BiOI Z-scheme photocatalyst with enhanced visible light photocatalytic activity, *J. Colloid Interface Sci.*, 2020, **576**, 34-46.
6. K. Ojha, T. Debnath, P. Maity, M. Makkar, S. Nejati, K. V. Ramanujachary, P. K. Chowdhury, H. N. Ghosh and A. K. Ganguli, Exciton separation in CdS supraparticles upon conjugation with graphene sheets, *J. Phys. Chem. C*, 2017, **121**, 6581-6588.
7. X. Yan, J. H. Dong, J. Y. Zheng, Y. Wu and F. X. Xiao, Customizing precise, tunable, and universal cascade charge transfer chains towards versatile photoredox catalysis, *Chem. Sci.*, 2024, **15**, 2898-2913.
8. X. C. Dai, M. H. Huang, Y. B. Li, T. Li, S. Hou, Z. Q. Wei and F. X. Xiao, Probing the advantageous photosensitization effect of metal nanoclusters over plasmonic metal nanocrystals in photoelectrochemical water splitting, *J. Phys. Chem. C*, 2020, **124**, 4989-4998.
9. S. Hou, X. C. Dai, Y. B. Li, M. H. Huang, T. Li, Z. Q. Wei, Y. H. He, G. C. Xiao and F. X. Xiao, Charge transfer modulation in layer-by-layer-assembled multilayered photoanodes for solar water oxidation, *J. Mater. Chem. A*, 2019, **7**, 22487-22499.
10. F. X. Xiao, Z. P. Zeng and B. Liu, Correction to "bridging the gap: electron relay and plasmonic sensitization of metal nanocrystals for metal clusters", *J. Am. Chem. Soc.*, 2015, **137**, 13990-13990.